J Therm Anal Calorim (2009) 98:105–111
DOI 10.1007/s10973-009-0451-3

Thermal and structural properties of binary mixtures of 1,3-distearoyl-2-oleoyl-glycerol (SOS) and 1,2-dioleoyl-3-stearoyl-*sn*-glycerol (*sn*-OOS)

L. Zhang · S. Ueno · K. Sato · R. O. Adlof · G. R. List

Special Chapter dedicated to the memory of dr. Michel Ollivon

Abstract We have conducted thermal and X-ray diffraction experiments on binary mixtures of symmetric stearic-oleic mixed-acid triacylglycerol (TAG) (1,3-distearoyl-2-oleoyl-glycerol: SOS) and asymmetric stearic-oleic mixed-acid TAG (1,2-dioleoyl-3-stearoyl-*sn*-glycerol: OOS), in which optically active *sn*-OOS was employed. We found that SOS–OOS mixtures exhibited immiscible monotectic or peritectic mixing behavior. This result was consistent with previous study on binary mixtures of 1,3-dipalmitoyl-2-oleoyl-glycerol (POP) and 1,2-dioleoyl-3-palmitoyl-*rac*-glycerol (OOP), in which racemic *rac*-OOP molecules were employed. The differences between the SOS–OOS and POP–OOP mixtures were in the polymorphic behavior of the fractions of POP and SOS. No effect was found from using an optically active (*sn*-OOS) or racemic mixture (*rac*-OOP) as an asymmetric oleic–oleic-saturated acid TAG. From the two results, we may conclude that an immiscible phase was formed in the binary mixtures of symmetric saturated-oleic-saturated TAGs and asymmetric oleic–oleic-saturated TAGs, of both racemic and optically active types. This result stands in contrast to mixtures of SOS–OSO (1,3-dioleoyl-2-stearoyl-glycerol), SOS–SSO (1,2-distearoyl-3-oleoyl-*rac*-glycerol), POP–OPO (1,3-dioleoyl-2-palmitoyl-glycerol), and POP–PPO (1,2-dipalmitoyl-3-oleoyl-*rac*-glycerol), all of which exhibited molecular-compound-forming behavior with molecular compound crystals at an equal ratio of the binary mixtures. Molecular-level mechanisms to explain this difference are discussed, based on possible roles of glycerol groups acting during the mixing processes of saturated–unsaturated mixed-acid TAGs.

Keywords Binary phase behavior · SOS · OOS · Polymorphism · DSC · X-ray diffraction

Introduction

The structural properties of TAG crystals are influenced by the molecular properties of TAGs, such as saturated/unsaturated fatty acid moieties, glycerol conformations, symmetry/asymmetry of the fatty acid compositions connected to the glycerol group, mixing behavior of different TAGs having different types of fatty acid moieties, etc. [1–3] Particular attention should be paid to saturated–unsaturated (Sat–Unsat) mixed-acid TAGs, since these TAGs are most abundantly present in vegetable oils and fats for edible applications [4, 5]. Understanding the phase behavior of binary mixtures of symmetric and asymmetric Sat–Unsat mixed-acid triacylglycerols (TAGs) have high significance for the separation of high-melting and low-melting fractions of vegetable fats and oils, and for texture control of fat-based food products such as margarine and chocolate [6–8]. In previous studies, the formation of a molecular compound has been observed in binary mixture systems of symmetric saturated–unsaturated mixed-acid TAGs, such as SOS–OSO [9], SOS–SSO [10, 11], POP–OPO [12], and POP–PPO [13]. However, our recent study found that the POP–OOP mixtures exhibited an immiscible eutectic nature, in both their metastable and most stable states [14].

L. Zhang
Zhengzhou University of Light Industry, Zhengzhou, China

S. Ueno · K. Sato (✉)
Graduate School of Biosphere Science, Hiroshima University, Hiroshima, Japan
e-mail: kyosato@hiroshima-u.ac.jp

R. O. Adlof · G. R. List
USDA, ARS, NCAUR, Peoria, IL, USA

In general, the molecular interactions that influence the mixing properties of TAGs containing saturated and unsaturated fatty acid chains are aliphatic chain packing, glycerol conformation, double-bond configuration, and methyl end stacking [6, 8, 15]. The formation of a double-chain-length structure in molecular compounds of POP–OPO and POP–PPO is due to the combined effects of the above molecular interactions between component TAGs. The inability to form a molecular compound in the POP–OOP mixture was explained by the influence of glycerol conformation and aliphatic chain packing. Further studies are required in order to clarify the molecular-level mechanisms of the phase behavior of binary mixture systems of symmetric and asymmetric saturated and unsaturated mixed-acid TAGs.

Most of the previous studies have been conducted using racemic asymmetric Sat–Unsat mixed-acid TAGs [11, 13, 14]. It should be interesting to examine a mixture of symmetric and asymmetric mixed-acid TAGs in which asymmetric TAGs are optically active molecules, not racemic molecules. In the present study, we used SOS and *sn*-OOS (*sn*: stereo-specifically numbered) to find whether the mixing behavior differs between two stereo isomers, and to understand how the mixing behavior exhibits either a molecular-compound forming or eutectic system. From a stereo-specific point of view, according to previous studies of optically active (S–) and racemic (RS–) α-monostearin crystals, an (RS)-form crystal is a racemic molecular compound consisting of (R–) and (S–) crystals [16]. Specifically, there is a eutectic point in the phase diagram between optically active (S–) and racemic (RS–) α-monostearin. Therefore, it is quite interesting to observe the binary mixing properties of symmetric Sat–Unsat TAGs and racemic or optically active asymmetric Sat–Unsat TAGs.

Differential scanning calorimetry (DSC) is a powerful instrument for the characterization of phase transition to determine the technological parameters of edible fats [17, 18]. DSC and high resolution X-ray diffraction coupling allows both thermal analysis and structural modifications analysis simultaneously [19]. In the present study, we conducted thermodynamic and kinetic studies of binary mixtures of SOS–*sn*-OOS using DSC and X-ray diffraction, with a conventional generator and synchrotron radiation. No molecular compound was observed in the metastable or stable states in the SOS–*sn*-OOS mixture, quite similar to the POP-*rac*-OOP mixtures. The absence of molecular-compound crystals in binary mixtures of POP–OOP and SOS–OOS is explained by taking into account the molecular interactions of acyl chain packing, glycerol conformation, and methyl end stacking, among which glycerol conformation appeared to be the most influential.

Materials and methods

SOS was purchased from Sigma Chemical Co. (St. Louis, MO) at 99% purity and used without further purification. *sn*-SOO was synthesized using a method based on Kodali's experiment [3]. Binary mixtures of SOS and OOS were prepared by mixing the weighted samples at room temperature, melting them above 50 °C, mixing using a vortex mixer, rapidly cooling to 0 °C, and then tempering at different temperatures. To obtain the most stable forms, thermodynamic equilibration was achieved by incubating the crystallized mixture samples at 20 °C for more than a month.

The transformation and melting behavior of the mixtures were measured by DSC (DSC-8240 and DSC-8230, Rigaku Co., Tokyo, Japan) at rates of 2 °C/min and 5 °C/min. Crystal forms in the most stable state were measured by powder X-ray diffraction (XRD) (RINT-TTR, Rigaku Co., Tokyo, Japan; $\lambda = 0.154$ nm) using a rotator-anode X-ray generator. Synchrotron radiation X-ray diffraction (SR-XRD, $\lambda = 0.150$ nm) was used to observe the kinetic processes of crystallization and melting in the metastable states using two beam lines, BL-9C and BL-15A, in the synchrotron radiation facility (known as the Photon Factory (PF)) at the High Energy Research Accelrator Research Organization (KEK) in Tsukuba, Japan. The PF operates at 2.5 GeV. X-ray diffraction patterns were recorded every 10 and 30 s using two gas-filled one-dimensional position-sensitive proportional counters that were placed for a small-angle region (Rigaku Co., Tokyo, Japan; 1024 channels over a total length of 200 mm) and a wide-angle region (Rigaku Co., Tokyo; 512 channels over a total length of 100 mm). The distance between the sample and the detector was 1,100 mm (small-angle) and 280 mm (wide-angle). The temperatures of the samples were changed with a Mettler DSC-FP84 (Columbus, USA) with a cooling rate of 5 °C/min. In special cases to observe kinetic processes of crystallization and melting in the metastable states, simultaneous synchrotron radiation X-ray diffraction and DSC measurements (SR-XRD/DSC) were used. With the use of a modified DSC (Mettler model FP84) and time-resolved XRD, thermal data for the cooling rate of 5 °C/min were obtained simultaneously from the same sample, as reported in detail elsewhere [20, 21].

Results and discussion

Phase behavior in the most stable state

DSC heating thermopeaks obtained at a rate of 2 °C/min for the most stable forms of the SOS–OOS mixtures at various concentration ratios of SOS/OOS are depicted in

Fig. 1. Single endothermic peaks were observed for pure OOS and SOS, corresponding to the melting temperatures of the β' form of OOS and the β form of SOS. Individual widened endothermic peaks of OOS appeared in the mixtures of SOS/OOS = 10/90 and 20/80. The second endothermic peak, indicated by arrow 1, was detectable from the mixture of SOS/OOS = 30/70 to 80/20 and increased in temperature and proportion with an increasing concentration of SOS, whereas the first melting peaks corresponding to the OOS fraction were weakened up to SOS/OOS = 80/20, as indicated by arrow 2, and disappeared in mixtures containing OOS concentrations of 10%.

Figure 2 presents a phase diagram constructed by summarizing the onset, offset, and peak temperatures encountered in the DSC experiments, defined as indicated in the box in Fig. 1. The polymorphic forms were determined by XRD measurements (see below). It is clear that SOS and *sn*-OOS are immiscible, revealing the monotectic mixing property, except for the concentration ranges for each component of less than 20–30%, where either minor component is incorporated as an impurity in crystalline phases of the major component. Within these narrow concentration ranges, the minor components were solubilized into the major components, since no specific DSC melting peaks of the minor components were detected. Therefore, the total phase behavior may be characterized as peritectic. The phase behavior of the SOS–*sn*-OOS mixtures in Fig. 2 was quite similar to that of POP-*rac*-OOP.

Figure 3 presents XRD patterns for the most stable forms of SOS–OOS binary mixtures, obtained by a rotator-anode

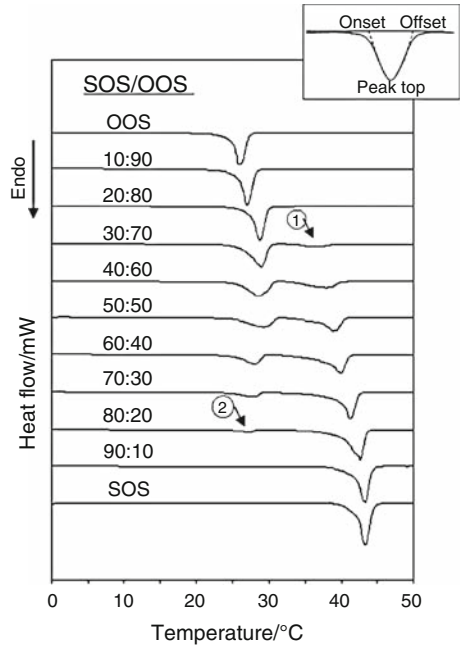

Fig. 1 DSC heating thermopeaks of SOS–*sn*-OOS mixtures in the most stable states

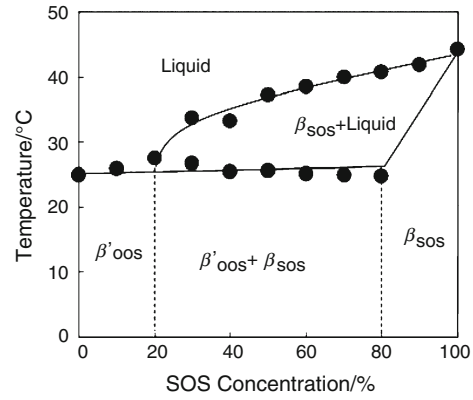

Fig. 2 Phase diagram of SOS–OOS mixture based on DSC melting profiles, with onset temperatures

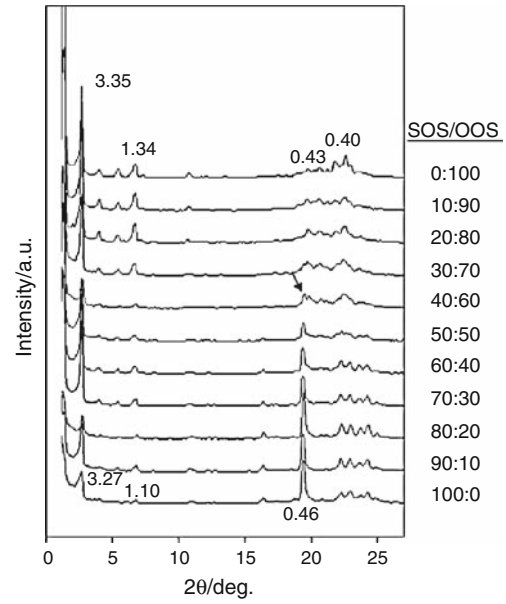

Fig. 3 X-ray diffraction patterns of the most stable states of the SOS–*sn*-OOS mixtures

X-ray generator. In small-angle diffraction areas, 001 reflections were not clearly detected, whereas 002 and higher-order reflections were. The pure OOS sample exhibited short spacing peaks at 3.35 nm (002 reflection) and 1.34 nm (005 reflection), and the pure SOS sample exhibited the same at 3.27 nm (002 reflection) and 1.10 nm (005 reflection). These data correspond to the long spacing values of 6.7 nm for OOS and 6.5 nm for SOS. The most stable polymorphic form of *sn*-OOS was the β' form, characterized by short spacing values of 0.40 and 0.43 nm. Pure SOS exhibited wide-angle X-ray diffraction (WAXD) peaks of the β form having a typical short spacing of 0.46 nm, corresponding to a triclinic parallel ($T_{//}$) subcell. The chain-length structure for β' of *sn*-OOS and β of SOS was assessed as triple because of the relative diffraction peaks of 002 and 005 reflections in the long-spacing patterns.

Mixing the SOS and *sn*-OOS samples produced no new peaks in SAXD patterns at any of the SOS/OOS ratios aside from those of the SOS and OOS fractions. The WAXD patterns exhibited a strong peak of 0.46 nm in the mixtures with SOS concentrations over 40%, marked by an arrow, indicating the occurrence of the β form of SOS. In the mixture with an SOS concentration of 30%, the peak at 0.46 nm was too weak to be clearly detected. With increasing SOS concentration, the intensity of the 0.46 nm peak increased, whereas the intensity of the 0.40 and 0.43 nm peaks decreased. Figure 2 summarizes the results of the XRD experiments on the occurrence of the β' form of OOS and the β form of SOS.

Phase behavior in the metastable state

Figure 4 plots the DSC heating thermopeaks of the metastable forms of SOS–*sn*-OOS mixtures, taken at a heating rate of 5 °C/min soon after the mixture samples were cooled from 50 to −20 °C at a cooling rate of 5 °C/min and held at −20 °C for 5 min. Figure 5 summarizes the kinetic phase behavior of the metastable forms, as constructed from the thermal data in Fig. 4. The quite complicated DSC thermopeaks and phase behavior seen in Figs. 4 and 5 can be understood by precisely observing the dynamics of the crystallization and transformation processes of the SOS and SOS fractions, examined using SR-XRD techniques. Due to limited space, we explain the SR-XRD data for pure OOS in Fig. 6, pure SOS in Fig. 7, and SOS/OOS = 50/50 in Fig. 8.

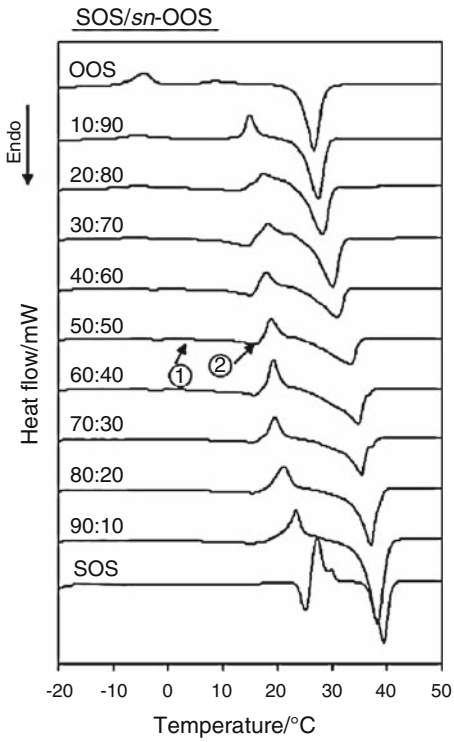

Fig. 4 DSC heating thermopeaks of the metastable forms of SOS–*sn*-OOS mixtures, measured at a heating rate of 5 °C/min

As seen in Fig. 4, the DSC heating study of pure *sn*-OOS exhibited a large, broad exothermic peak around −5 °C, a small exothermic peak around 8 °C, and a sharp endothermic peak at 27 °C. Figure 6 presents SR-XRD patterns for *sn*-OOS, taken during cooling and heating between 35 and −20 °C, varying at 5 °C/min. At −20 °C, isothermal treatment was conducted for 10 min before heating. During the cooling process, the α form, with long spacing peaks at 6.0 nm (001 reflection) and 3.0 nm (002 reflection) and a short spacing peak at 0.42 nm, occurred at −4.4 °C. On heating, the α form transformed to the β' form, with a long spacing of 6.74 nm (001 reflection) and 3.37 nm (002 reflection) and short spacings of 0.43 and 0.39 nm between −10 and 0 °C. This transformation

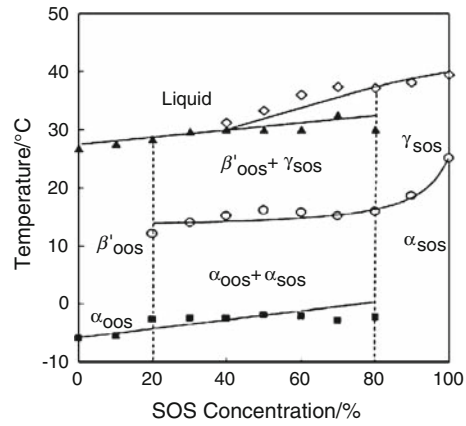

Fig. 5 Kinetic phase behavior of SOS–*sn*-OOS mixtures

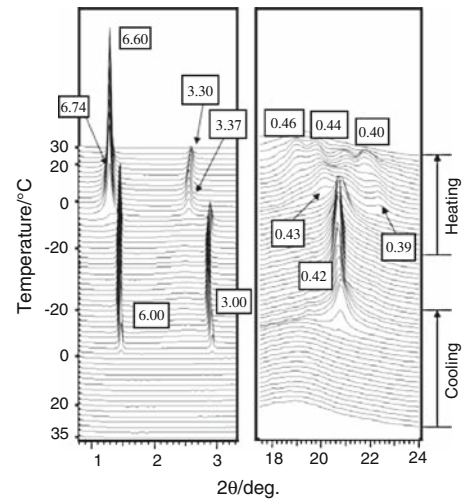

Fig. 6 Synchrotron radiation XRD patterns of crystallization, transformation, and melting of metastable forms of *sn*-OOS, taken during cooling and heating between 35 and −20 °C at a rate of 5 °C/min

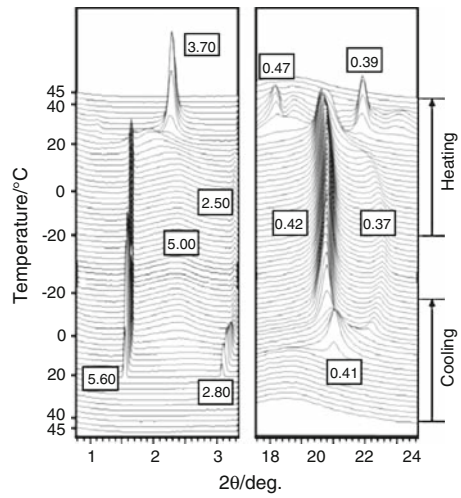

Fig. 7 Synchrotron radiation XRD patterns of crystallization, transformation, and melting of metastable forms of SOS, taken during cooling and heating between 45 and −20 °C at a rate of 5 °C/min

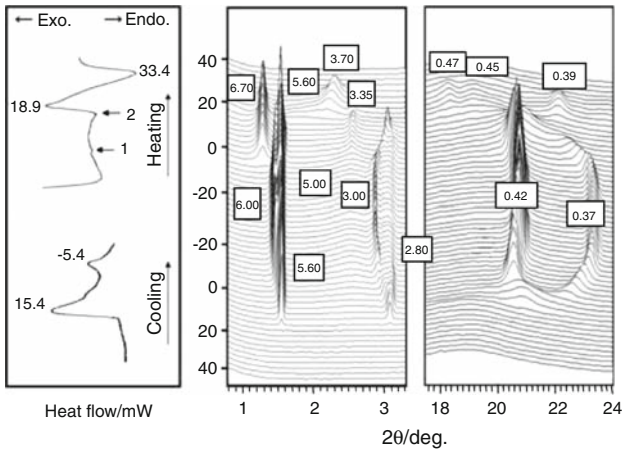

Fig. 8 DSC/SR-XRD patterns of meta-stable forms of the SOS/*sn*-OOS = 50/50 mixtures, taken at a rate of 5 °C/min. The lattice parameter values are noted only for major peaks

corresponds to a broad exothermic peak in the DSC pattern for *sn*-OOS in Fig. 4, around −5 °C. Around 8 °C, the long-spacing peaks changed to 6.60 nm (001 reflection) and 3.30 nm (002 reflection), and the short-spacing peaks changed to 0.46, 0.44, and 0.40 nm, corresponding to the broad exothermic peak in Fig. 4. We think that this transformation is from β'_2 to β'_1 of *sn*-OOS and that further heating caused the melting of β'_1 around 27 °C.

Figure 4 plots the DSC heating thermopeaks of pure SOS, with a sharp endothermic peak at 25 °C followed by a sharp exothermic peak at 27 °C, and with an endothermic peak appearing at 39.4 °C. Figure 7 presents SR-XRD patterns taken during cooling and heating between 45 and −20 °C, varying at a rate of 5 °C/min. During cooling, an α form with long-spacing peaks of 5.60 nm with 001 reflection (5.60 nm) and 002 reflection (2.80 nm) and a short-spacing peak of 0.41 nm first occurred around 20 °C. On further cooling, the α form transformed into a sub-α form with long-spacing peaks of 5.00 nm with 001 reflection (5.00 nm) and 002 reflection (2.50 nm) and short-spacing peaks of 0.42 and 0.37 nm at 3 °C. The long-spacing values indicate that the two forms are double-chain-length structures. On heating, the transformation from sub-α form to α form occurred at 7 °C, as typically indicated by the disappearance of the short-spacing peak of 0.37 nm of the sub-α form. Around 27 °C, the long- and short-spacing peaks of the α form disappeared, and a long-spacing peak of 3.70 nm (002 reflection) and short-spacing peaks of 0.47 and 0.39 nm appeared. These peaks are characteristic of the γ form of SOS, a triple-chain-length structure. This conversion from α form to γ form corresponded to a melt-mediated transformation, in which an endothermic peak due to melting of the α form is associated with an exothermic peak due to crystallization of the γ form in the DSC patterns in Fig. 4. Further heating caused the disappearance of the XRD patterns of the γ form at around 40 °C.

Table 1 summarizes the long- and short-spacing values for the polymorphic forms of pure SOS and *sn*-OOS.

In the mixtures with SOS/OOS = 30/70, 40/60, 50/50, 60/40, and 70/30, concurrent crystallization of the SOS and *sn*-OOS fractions was clearly observed by SR-XRD, which indicated the crystallization and transformation of SOS and *sn*-OOS fractions with their immiscible mixing nature. Here, we describe the results of the SOS/OOS = 50/50 mixture in detail.

Figure 8 presents simultaneous DSC/SR-XRD patterns of the SOS/OOS = 50/50 mixtures, taken by cooling and heating between 40 and −20 °C with isothermal treatment for 10 min at −20 °C before heating. During cooling, the α form of SOS with its long-spacing peak at 5.6 nm and short spacing-peak of 0.41 nm first crystallized around 15.4 °C. After that, the α form of OOS, having long-spacing peaks at 6.0 nm (001 reflection) and 3.0 nm

Table 1 Typical long and short spacing values of polymorphic forms of SOS and *sn*-OOS

Triacylglycerols	Long spacing/nm	Short spacing/nm
SOS		
Sub-α form	5.00	0.42, 0.37
α form	5.60	0.41
γ form	7.40	0.47, 0.39
β form	6.50	0.46
sn-OOS		
α form	6.00	0.42
β'_2 form	6.74	0.43, 0.39
β'_1 form	6.60	0.46, 0.44, 0.40

(002 reflection) and a short-spacing peak at 0.42 nm crystallized at −5.4 °C, and the α form of the SOS fraction transformed to sub-α form. In the temperature range of −5 to 5 °C during heating, the α form of OOS melted and transformed into β', as indicated by the occurrence of long-spacing peaks at 6.7 nm (001 reflection) and 3.35 nm (002 reflection) at the expense of the peaks at 6.0 and 3.0 nm. The sub-α form of the SOS fraction transformed into α and γ forms, as evidenced by the variation in the long-spacing peaks from 5.0 to 5.6 nm and 3.7 nm. The first small endothermic peak around −2 °C in the DSC patterns, indicated by arrow 1 in Figs. 4 and 8, corresponds to the melting of the α form of the OOS fraction. The second endothermic peak around 16 °C, indicated by arrow 2 in Figs. 4 and 8, was due to melting of the α form of the SOS fraction. The large exothermic peak around 18–19 °C in Figs. 4 and 8 corresponds to the simultaneous occurrence of the β' form of OOS and the γ form of SOS, and the broad endothermic peak around 30–33 °C corresponds to their melting profiles. In the SOS–OOS mixture, it was difficult to determine β'_1 or β'_2 of OOS due to unclear long- and short-spacing peaks appearing in complicated diffraction patterns. As a characteristic of the γ form of SOS, the short-spacing peaks at 0.47, 0.45, and 0.39 nm as well as the long-spacing peak at 3.73 nm disappeared at around 34 °C.

The DSC-SR-XRD patterns for the SOS/OOS = 30/70, 40/60, 60/40, and 70/30 mixtures, although not shown here, were quite similar to those for SOS/OOS = 50/50 except for the difference in intensity of the SR-XRD patterns for the SOS and OOS fractions, caused by their relative concentration variations. Taking into account all of the SR-XRD patterns for the SOS–OOS mixtures with different SOS–OOS ratios, we determined the immiscible phase behavior for the meta-stable polymorphisms of α, β', and γ of SOS and *sn*-OOS (Fig. 5).

Figure 9 presents a hypothetical structural model of a molecular compound of SOS and *sn*-OOS, illustrating that there would be difficulty either in arranging the glycerol groups or with lateral chain packing of stearic and oleic acid moieties, if we draw the molecular compound crystal as a double-chain-length structure. In model (1), the arrangements of the glycerol groups may have a discrepancy in the directions of the glycerol groups, as denoted by arrows, although the oleic acid and stearic acid moieties are packed in separated leaflets. In model (2), however, the aliphatic chain packing may have steric hindrance because of the coexistence of stearic acid and oleic acid chains in each leaflet, although the glycerol groups are well arranged. Therefore, it is difficult to construct a molecular compound crystal with SOS and *sn*-OOS. The same argument was applied to the binary mixture systems of POP-OOP in our previous study, although racemic molecules of OOP were employed [14].

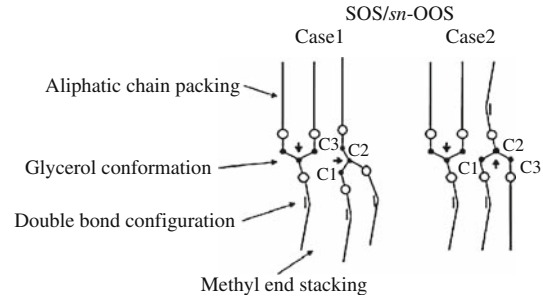

Fig. 9 Structural models illustrating glycerol groups of a hypothetic molecular compound structure of SOS–*sn*-OOS

To summarize, the polymorphic behavior of SOS–*sn*-OOS mixtures resulted in the following. (i) There is no molecular compound for an SOS/*sn*-OOS mixture, and SOS–OOS mixtures are immiscible, in both the metastable and most stable polymorphic systems. (ii) A time-resolved SR-XRD study revealed the polymorphic occurrence of a binary mixture in the metastable states. In contrast to POP–OOP mixtures, in which the POP fraction transformed from α to β' with no passage through γ in the presence of OOP, the SOS fraction transformed as $\alpha \rightarrow \gamma \rightarrow \beta'$. (iii) A sub-α form appeared in the mixtures of SOS–*sn*-OOS, whereas no sub-α form occurred in the POP fraction in the POP–OOP mixture. By combining the results of studying the mixing phase behavior of SOS–*sn*-OOS and POP-rac-OOP, we may conclude that an immiscible phase is formed in binary mixtures of symmetric saturated-oleic-saturated TAGs and asymmetric oleic–oleic-saturated TAGs of both the racemic and optically active types.

References

1. Sato K. Solid-state behaviour of polymorphic fats and fatty acids. In: Larsson K, Quinn P, Sato K, Tiberg F, editors. Lipids: structure, physical properties and functionality. Bridgewater, UK: The Oily Press; 2006. p. 9–72.
2. Small DM. Glycerides. In: Small DM, editor. The physical chemistry of lipids from alkanes to phospholipids. New York: Plenum Press; 1988. p. 345–94.
3. Kodali DR, Atkinson D, Redgrave TG, Small DM. Synthesis and polymorphism of 1,2-dipalmitoyl-3-acyl-sn-glycerols. J Am Oil Chem Soc. 1984;61:1078–84.
4. Timms RE. Phase behaviour of fats and their mixtures. Prog Lipid Res. 1984;23:1–67.
5. Sato K, Ueno S. Polymorphism in fats and oils. In: Shahidi F, editor. Bailley's, industrial oil & fat products, vol. 1. New Jersey: Wiley; 2005. p. 77–120.
6. Sato K, Ueno S, Yano J. Molecular interactions and kinetic properties of fats. Prog Lipid Res. 1999;38:91–116.
7. Marangoni AG. Crystallography. In: Marangoni AG, editor. Fat crystal networks. New York: Marcel Dekker; 2005. p. 1–21.
8. Timms RE. Physical chemistry. In: Timms RE, editor. Confectionery fats handbook, properties, production and application. Bridgewater, UK: The Oily Press; 2003. p. 110–9.

9. Koyano T, Hachiya I, Sato K. Phase behavior of mixed systems of SOS and OSO. J Phys Chem. 1992;96:10514–20.
10. Engstrom L. Triglycerides systems forming molecular compounds. J Fat Sci Technol. 1992;94:173–81.
11. Takeuchi M, Ueno S, Sato K. Crystallization kinetics of polymorphic forms of a molecular compound constructed by SOS (1,3-distearoyl-2-oleoyl-sn-glycerol) and SSO(1,2-distearoyl-3-oleoyl-rac-glycerol). Food Res Int. 2002;35:919–26.
12. Minato A, Ueno S, Yano J, Smith K, Seto H, Amemiya Y, et al. Thermal and structural properties of sn-1,3-dipalmitoyl-2-oleoylglycerol and sn-1,3-dioleoyl-2-palmitoylglycerol binary mixtures examined with synchrotron radiation X-ray diffraction. J Am Oil Chem Soc. 1997;74:1213–9.
13. Minato A, Ueno S, Smith K, Amemiya Y, Sato K. Thermodynamic and kinetic study on phase behavior of binary mixtures of POP and PPO forming molecular compound systems. J Phys Chem B. 1997;101:3498–505.
14. Zhang L, Ueno S, Miura S, Sato K. Binary phase behavior of 1,3-dipalmitoyl-2-oleoyl-sn-glycerol and 1,2-dioleoyl-3-palmitoyl-rac-glycerol. J Am Oil Chem Soc. 2007;84:219–27.
15. Sato K, Ueno S. Molecular interactions and phase behavior of polymorphic fats. In: Garti N, Sato K, editors. Crystallization processes in fat and lipid systems. New York: Marcel Dekker; 2005. p. 177–210.
16. Iwahashi M, Watanabe Y, Muramatsu M, Muramatsu M. Optically active and racemic glycerides.I. The thermodynamic and structural relationship between optically active and the corresponding racemic α-monostearins in their crystalline, molten, and dissolved states. Bull Chem Soc Jpn. 1984;57:1446–8.
17. Lõrinczy D, Regdon G, Keller B, Szakály S, Schäffer B. Development of certain technological parameters of margarine and mixed-fat spread. J Therm Anal Calorim. 2007;88:2351–4.
18. Lopez C and Ollivon M. Crystallization of triacylglycerols in nanoparticles. Effect of dispersion and polar lipids. J Therm Anal Calorim. 2009; doi:10. 1007/s10973-009-0183-4.
19. Ollivon M, Keller G, Bourgaux C, Kalnin D, Villeneuve P, Lesieur P. DSC and high resolution X-ray diffraction coupling. J Therm Anal Calorim. 2006;85:1219–24.
20. Ueno S, Hamada Y, Sato K. Controlling polymorphic crystallization of n-Alkane crystals in emulsion droplets through interfacial heterogeneous nucleation. Cryst Growth Des. 2003;3:935–9.
21. Higami M, Ueno S, Segawa T, Iwanami K, Sato K. Simultaneous synchrotron radiation X-ray diffraction-DSC analysis of melting and crystallization behavior of trilauroylglycerol in nanoparticles of oil-in-water emulsion. J Am Oil Chem Soc. 2003;80:731–9.